Received 11 July 2023, accepted 1 August 2023, date of publication 7 August 2023, date of current version 14 August 2023.

Digital Object Identifier 10.1109/ACCESS.2023.3302889

RESEARCH ARTICLE

Precise 2D and 3D Fluoroscopic Imaging by Using an FMCW Millimeter-Wave Radar

YAHENG WANG, JIE SU, TAIGA FUKUDA, MASAYOSHI TONOUCHI, (Member, IEEE), AND HIRONARU MURAKAMI

Institute of Laser Engineering, Osaka University, Osaka 565-0871, Japan

Corresponding author: Hironaru Murakami (murakami.hironaru.ile@osaka-u.ac.jp)

This work was supported in part by the Japan Society for the Promotion of Science (JSPS) KAKENHI under Grant JP22H01550.

ABSTRACT This study utilized a multiple-input multiple-output synthetic aperture radar (MIMO-SAR) technology employing a frequency-modulated continuous wave (FMCW) millimeter-wave MIMO radar to execute two-dimensional (2D) and three-dimensional (3D) imaging of objects. By analyzing the intermediate frequency (IF) signal generated from the transmitted and received chirp signals, Range FFT spectra with information on the distance to the object and on the reflection intensity according to frequency were obtained. The integration of reflection intensity provided a comprehensive image at varying distances, while the 2D cross-sectional image of an object inside a concealed cardboard achieved a spatial resolution of less than 1 mm. Through innovative data processing techniques, such as the spatial translation filter, we succeeded in the reconstruction of a monolayered 3D image of a clothed human body's surface. Moreover, the system demonstrated its potential for security checks by effectively identifying dangerous items concealed by human.

INDEX TERMS Chirp radar, imaging, millimeter wave radar, MIMO, synthetic aperture radar.

I. INTRODUCTION

Electromagnetic waves within the frequency range of 30-300 GHz are commonly referred to as millimeter waves (MMWs) due to their corresponding wavelengths ranging from 10 mm to 1 mm. MMWs have garnered significant attention in scientific research due to their distinctive properties. The utilization of MMWs in imaging applications has emerged as a compelling alternative to conventional measurement methods, offering potential solutions to their inherent limitations. One notable characteristic of MMWs is their high transmittance through various objects, including clothing and cardboard. This feature enables imaging through obstacles that hinder visibility in traditional measurement techniques. Furthermore, unlike other radiation-based methods, MMWs pose no risk of exposure, making them safer for both operators and subjects. Additionally, MMWs exhibit exceptional weather resistance, remaining functional even in adverse weather conditions such as rain and fog. These inherent advantages have led to the development of several applications utilizing MMWs for different purposes, including vehicle-mounted radar for driver assistance systems and automated driving [1], [2], biometric monitoring technology for non-contact measurement of vital signs [3], [4], [5], infrastructure inspection for detecting cracks under the lining paint [6], [7], [8], [9], non-destructive testing for object defect detection [10], [11], [12], security technology for the detection of dangerous objects [13], [14], [15].

The objective of this study is to perform various security and body checks in a non-contact manner, and it is crucial to advance measurement and data-processing technologies capable of obtaining high-precision, 3D information about object shapes accurately. Meanwhile, in order to expand the potential of this research for future practical applications, it is important that the system is compact as well as cost-effective.

However, a traditional MMW radar system consists of discrete components, including antenna components for transmission and reception, analog components for the clock, and digital components such as an A/D converter (ADC), microcontroller (MCU), and digital signal processor (DSP). Unfortunately, these discrete implementations result in larger

The associate editor coordinating the review of this manuscript and approving it for publication was Sukhdev Roy.

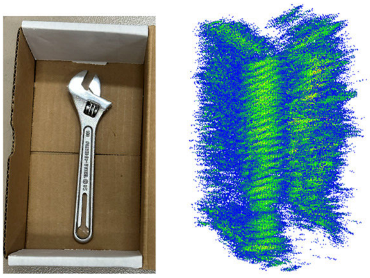

(a) (b)

FIGURE 1. (a) The image sample. (b) 3D imaging result.

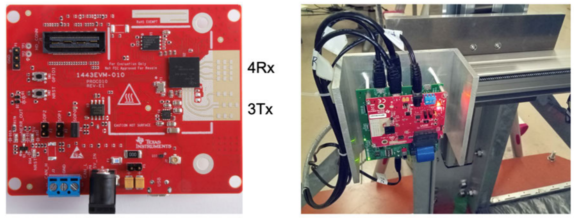

(a) (b)

FIGURE 2. (a) IWR1443 MMW module. (b) MMW imaging system.

and more complex systems, increased power consumption, and higher overall costs [16].

Despite the advancements in complementary metal-oxide semiconductor (CMOS) technology that have led to the integration of cost-effective MMW wideband radar sensors, the inherent challenge of requiring a significant number of sensors to achieve a comprehensive high-resolution image of the scene persists as a significant hurdle for MMW imaging systems [17], [18], [19].

In the related study on 3D MMW imaging, a 3D point cloud of metal springs utilizing a PR2 robot for 3D geometric imaging has been successfully constructed [20], this work used a vector network analyzer to transmit MMWs at 15 - 26.5 GHz, and the distance resolution of approximately 13.6 mm. While using radar with a wider bandwidth could slightly improve the distance resolution, it is not an optimal choice in terms of system compactness and price. On the other hand, Texas Instruments has developed a single-board FMCW MMW radar module (model: IWR1443) with continuous frequency modulation (77-81 GHz), which features a small size and low cost [21]. By utilizing this module, a compact MMW imaging system can be built to achieve a more effective and cost-efficient solution. A previous study proposed a 3D image reconstruction algorithm using MMW multiple-input multiple-output (MIMO) radar. Nevertheless, the visibility of the reconstructed images was severely affected by the lack of proper data processing for achieving 3D imaging of object contours. For instance, when the wrench was measured within a cardboard box, as shown in Fig.1 (a), the resulting 3D image suffered from significant noise interference caused by the cardboard and the surrounding environment. This led to the inability to accurately recognize the wrench as intended, as shown in Fig.1 (b). Additionally, almost all previous studies focused on measuring objects with flat surfaces, with few results on objects with curved surfaces [21], [22]. Because the reflected signal from an object with curved surfaces (e.g., the human body) is quite weak [23].

Therefore, the purpose of the present study is to involve processing the observed point cloud data to faithfully reproduce the 3D shapes of various original objects. The novelty and significant contribution of this study lies in the successful implementation of our innovative image reconstruction techniques, enabling the accurate reproduction of the 3D shape of a non-planar object. Notably, our techniques achieve an impressive spatial resolution of less than 1 mm, both in-plane and at a distance. Furthermore, our focus in future research will be on enhancing the algorithm for point cloud data to achieve better resolution and incorporating deep learning for object recognition of 2D and 3D point clouds.

II. MILLIMETER-WAVE FMCW RADAR SYSTEM

In this work, the IWR1443 module, depicted in Fig. 2(a), was attached to a 2-axis mechanical stage for X-Z scanning purposes, as shown in Fig.2 (b). The duration of the chirp signal in the 77-81 GHz range is 40 μs. The received signal reflected from an object of the measurement target is mixed with the transmitted signal by a mixer, and the frequency components of the sum and difference of the two signals are output [24]. By passing this mixed signal through a low-pass filter (LPF), only the difference frequency component is extracted as an intermediate frequency (IF) signal [25], [26]. Using the IF signal, we can obtain a Range FFT spectrum in which each spectrum peak reflects the position of the object's surfaces. Hence, it is possible to obtain reconstructed 2D and 3D images using the point cloud data corresponding to the object's distance in the Y-direction.

To achieve high spatial resolution in our system, we employ MIMO-SAR (Synthetic Aperture Radar) technology, which reduces hardware complexity and cost. MIMO is a communication technology employing multiple transmit (Tx) and receive (Rx) antennas. These antennas were positioned at regular intervals based on the wavelength of the frequency used, thereby creating a virtual array that capitalizes on the phase differences in received signals [27]. This methodology aims to increase the effective radar aperture length and improve spatial resolution. To overcome the limitations of aperture length in MIMO technology, SAR technology has been integrated [28], [29], [30]. SAR utilizes the concept of a virtual orbit, wherein a large number of antennas are distributed along the radar system's path, allowing signal transmission and reception while the system is in motion [31], [32]. This dynamic movement effectively increases the aperture length, thus enhancing system performance.

Moreover, the distance resolution is also important for an FMCW radar. Distance resolution is the capability of the radar to distinguish or resolve nearby adjacent objects in the

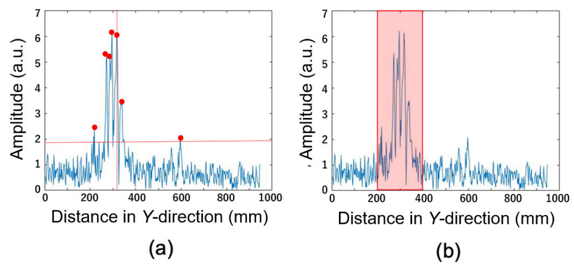

FIGURE 3. Different methods to obtain 2D images. (a) Cross-section method. (b) Distance-integrated method.

range, it can be calculated as follows [25]:

$$\Delta r = \frac{c}{2B} \tag{1}$$

where c is the speed of light and B is the sweep bandwidth. For the proposed MMW radar system, the sweep range is 77 - 81 GHz, by substituting the bandwidth $B =$ 4GHz into (1), we get that the theoretical distance resolution is about 3.75 cm. Owing to the sweep bandwidth of the device, enhancing the distance resolution remains unattainable. Therefore, our primary emphasis will be directed toward the processing of the observed point cloud data, to faithfully replicate the 3D shape of the object.

III. RECONSTRUCTION METHODS

This study employed the analysis of the Fourier-transformed IF signal to determine the reflection intensity at various distances, enabling 2D and 3D imaging. Ideally, the reflected intensity data obtained through the analysis of the IF signal should exhibit a single intensity peak corresponding to the distance from the object of measurement [25]. However, in practice, this outcome is influenced by factors such as the strength of the chirp signal utilized, environmental noise, and micro-motion or vibrations originating from the object itself [14]. Moreover, the measurement process involves mounting the MMW module on a two-axis stage that moves in 2D during the measurement, thereby introducing vibrations as an inevitable interference. Consequently, it is uncommon to obtain a single intensity peak when analyzing the reflected signal from an object of measurement target.

There are several methods for obtaining 2D reconstructed images from a Rang FFT spectrum [33], [34], and we obtained (i) 2D cross-sectional and (ii) integral images in the following ways. (i) The Y-coordinates of the peaks giving intensities above a certain threshold are extracted from the Rang FFT (distance FFT) spectrum [see Fig. 3(a)] to create 3D point cloud data, and then a 2D cross-sectional image of the X-Z plane was obtained at each distance (Y). (ii) An integral image was obtained by determining the interval on the distance (Y) where the signal intensities were to be integrated and adding all the signal intensities within that interval together, as shown in Fig. 3(b).

The former approach enables imaging of objects within a particular section, but it possesses the drawback of being unable to capture the complete object if it is tilted or has a non-flat surface. Conversely, the latter approach allows for imaging objects at varying distances, presenting objects at a specific distance as a whole, akin to the perspective provided by a camera. Therefore, the spatial resolution of the system can be determined more successfully by analyzing cross-sectional images of objects with flat surfaces, and the overall fluoroscopic imaging of the object can be observed more successfully by analyzing integral images.

Acquiring a 2D image allows for determining the resolution of the internal cross-section, while the external contour of the object requires 3D imaging to obtain it. In previous studies, MMW imaging primarily concentrated on measurements of flat objects [35], [36]. However, the presence of environmental noise and object vibrations, besides device-specific distance resolution, often results in the emergence of multiple peaks around the object distance. Consequently, obtaining the outer contour of the object becomes exceptionally challenging. In order to obtain highly precise 3D point cloud coordinates, this study employed the same method as the previously mentioned (i), where the Y coordinates of peaks above a certain percentage (e.g., 70∼90%, depending on the object) near the peak intensity maximum (in close proximity to the object) were extracted to obtain the 3D point cloud data, as shown in Fig. 3(a). Consequently, for an (X, Z) coordinate, there have multiple Y values, as shown in Fig. 1(b). For 3D imaging utilizing point cloud data, it is crucial that the data accurately represents the external outline of the object. Therefore, for the data with multiple Y values in single (X, Z) coordinates, we developed the following 3D reconstruction algorithm.

The first step involved clustering the data based on their similarity. During the scanning process, background objects such as absorbers or metal supports may be present around the target objects. Hence, it was necessary to cluster the point clouds belonging to different objects to separate the point cloud of the object. The clustering equation used was as follows:

$$d = \sqrt{(x_1 - x_2)^2 + (y_1 - y_2)^2 + (z_1 - z_2)^2} \tag{2}$$

where d represents the distance between two points (x_1, y_1, z_1) and (x_2, y_2, z_2). If d is greater than a certain value, the two points are considered to belong to different groups, while if d is smaller than a certain value, the two points are considered to belong to the same group. By applying this clustering process, the point cloud of the sample could be separated. In this study, d was set at 5 mm.

The second step is to monolayer the point cloud of the sample. As previously mentioned, after preliminary filtering of the point cloud data, each (X, Z) coordinate had multiple Y values. Therefore, the average of all the Y values corresponding to the same (X, Z) point was calculated, and each (X, Z) coordinate corresponds to only one Y value. This step aimed to average out unnecessary thickness information and filter noise caused by environmental noise and vibrations of the object.

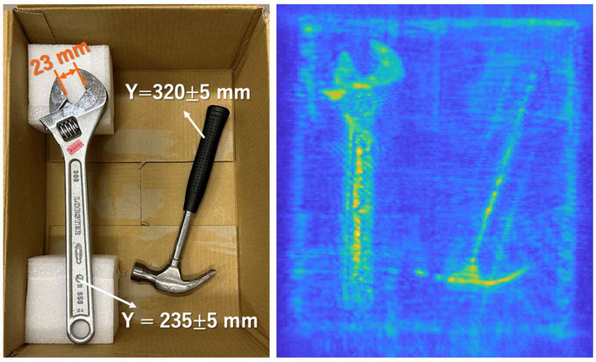

(a) (b)

FIGURE 4. **(a) Invisible wrench and hammer packed in a cardboard box. (b) 2D intensity integration image.**

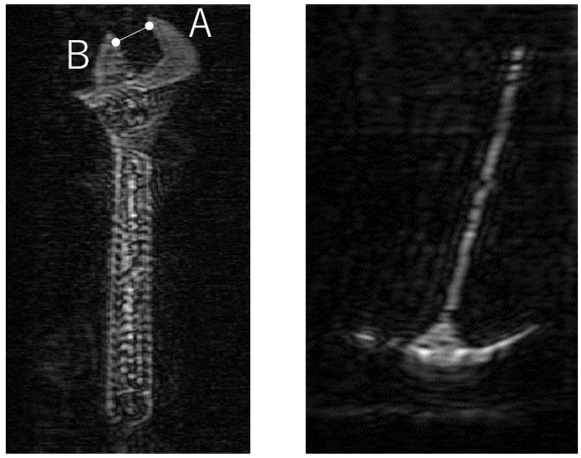

(a) (b)

FIGURE 5. **2D cross-sectional images. (a) Y = 237 mm. (b) Y = 322 mm.**

In the third step, 3D averaging was applied to the monolayered point cloud. After the second step, although each (X, Z) point only had one corresponding Y value, there was still a difference in the point clouds along the Y direction, making it difficult to obtain a smooth 3D result. To address this issue, 3D averaging was applied to the point cloud around a point (x_o, y_o, z_o) using the following equation:

$$\sqrt{(x_k - x_0)^2 + (y_k - y_0)^2 + (z_k - z_0)^2} \leq r^2 \tag{3}$$

$$\left(x_0', y_0', z_0'\right) = \frac{\sum_{k=1}^{N} (x_k, y_k, z_k)}{N} \tag{4}$$

Here, to process the 3D point cloud data, a sphere with a radius r was defined using a selected point (x_o, y_o, z_o) as the center. Within this sphere, all points (x_k, y_k, z_k) were extracted. The average of these N points was then calculated, and the resulting average coordinates were assigned as the new coordinates for the point $\left(x_0', y_0', z_0'\right)$. This process was performed for each point in the point cloud. In this study, this process was repeated 10 times with a gradually decreasing r value. This choice of radius allowed for an effective averaging of the nearby points within the defined sphere and contributed to generating smoother 3D results.

IV. IMAGING RESULTS

In order to measure the imaging performance of this MMW imaging system, and the accuracy of the data processing algorithms mentioned in the previous section, a wrench, and a hammer were packed inside a cardboard box as an imaging sample, which is depicted in Fig. 4 (a). To ensure stability, foam cushioning material was used to fix the tools within the boxes. The approximate distances of the wrench and hammer were at $Y = 235 \pm 5$ mm and $Y = 320 \pm 5$ mm from the MMW module, respectively. Furthermore, the length of open space between the fixed and movable jaws of the wrench was 23 mm. Fig.4 (b) presents a 2D intensity integration image displaying the reflection intensity in the depth direction (Y) at each (X, Z) coordinate within the range of $Y = 190 \sim 350$ mm. The intensity integration images effectively capture the wrench and hammer, despite their different depth positions along the Y-axis.

Furthermore, Fig. 5(a) and (b) show 2D cross-sectional images of the wrench and hammer at $Y = 237$ mm and $Y = 322$ mm, respectively. The 2D cross-sectional images show good spatial resolution in the X-Z plane and the accuracy of the imaging precisely. The moving parts of the wrench and hammer are clearly imaged at their respective placement locations. To assess the accuracy of the measurement using this data, the distance between points A and B is calculated in Fig. 5(a) based on the coordinates of two points, resulting in a value of 23.5 mm. In comparison, the actual distance between the fixed and movable jaws, as measured by calipers, is 23 mm. Incidentally, the interval between the measurement data along the X and Z axis $\Delta X_{min} = \Delta Z_{min} = 0.9$ mm. These results indicate that the MIMO-SAR imaging technique successfully achieves a measurement accuracy of less than 1 mm, accurately imaging the 2D plane represented in the 2D image.

The front view of the 3D point clouds of the wrench and hammer inside the cardboard box is shown in Fig. 6(a). The noise due to reflections from the area around the measurement chamber was eliminated beforehand and the signals which have weak reflected intensity have been removed. Fig. 6(b) shows the reconstructed 3D point cloud image, the red point cloud is the wrench, the orange point cloud is the hammer, and the blue point cloud represents the front and back of the box. By comparing these two point cloud images, we can conclude that the algorithm we developed effectively removes noise and the processed 3D point cloud accurately reconstructed the surface shape and position of the wrench and hammer in 3D space.

Furthermore, we conducted object scanning from four distinct directions at 90-degree intervals. The acquired data was then reconstructed, and the results from each direction were stitched together, considering the respective scanning angles.

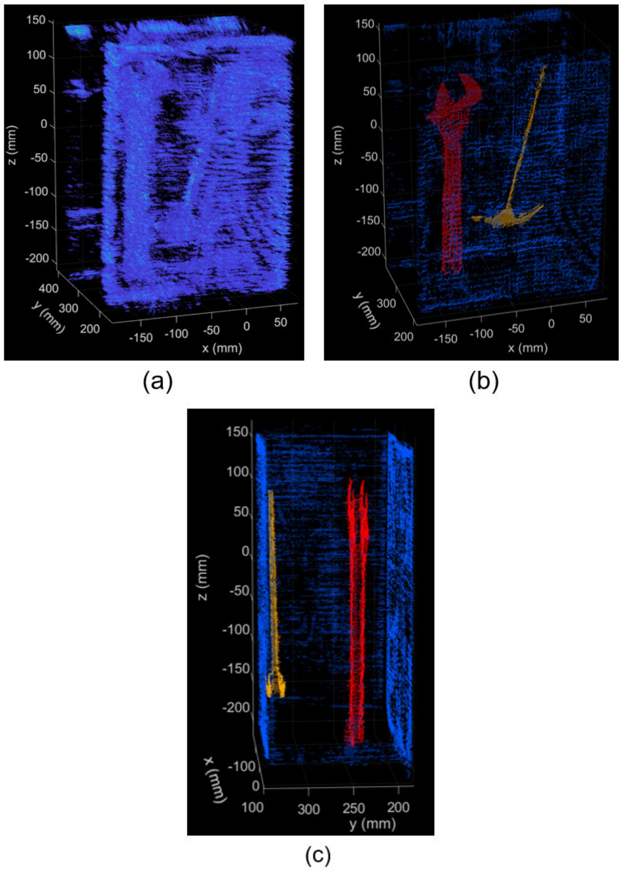

FIGURE 6. (a) 3D point cloud image after extracted peak intensity. (b) Reconstructed 3D point cloud image in one direction. (c) Reconstructed 3D point cloud image in four directions.

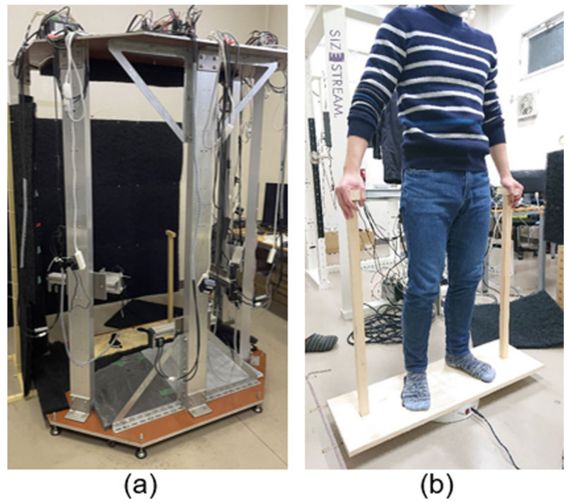

FIGURE 7. (a) Multi-angle MMW scanning system. (b) Clothed human standing on a precision turntable.

The supplementary video showcases rotated 3D imaging results [37], with a side view depicted in Fig. 6(c). It can be concluded that after reconstructing and stitching the point cloud data by scanning from multiple angles, the surface contour, and the position of the object in space are well restored.

In addition, in Fig. 6(c), the distance between the surface reflections from the wrench and the hammer in the Y-direction is 85.52 mm, which closely matches the practical distance. And the thickness of the wrench is determined to be 15.84 mm, which is quite similar to the actual thickness of 15 mm. This observation leads to the conclusion that the data processing algorithm employed in this paper achieves a distance resolution accuracy of less than 1 mm within the processed 3D point cloud.

V. HUMAN BODY MEASUREMENTS

MMWs exhibit excellent clothing penetration capabilities, making them highly suitable for security inspections involving the detection of dangerous objects. Previous research on human body detection has primarily focused on 2D imaging of a single side of the human body [15], [21], [22]. In this study, we have developed a data processing algorithm that allows us to acquire point cloud data representing the surface shape of the objects. However, it is important to note that the intensity of the reflection signal is extremely reduced as the angle of incidence deviates from the vertical while maintaining relatively high levels when the MMWs emitted from the module are injected and reflected at angles close to the vertical [38]. To address this issue, we have designed a multi-angle MMW scanning system, depicted in Fig. 7(a), which incorporates four MMW modules mounted on four two-axis mechanical stages. This configuration enables simultaneous scanning at four different angles, with an angular separation of 45 degrees between each module.

For the measurements of human body surfaces, a clothed human stood on a precision turntable positioned at the center of the multi-angle MMW scanning system. Furthermore, the wooden fixation bars were placed on either side of the body to prevent the body from moving too much, as presented in Fig. 7(b). Under these conditions, measurements were taken in 22.5-degree increments from around the human body. In other words, a total of four 2D scanning were carried out in a total measurement time of 16 minutes (4 minutes/scan). The 2D scanning in the present system involves repeated scanning in the horizontal (X-axis) direction at a speed of 500 mm/s, but if this is changed to a repeated scanning method in the vertical (Z-axis) direction and a system with 16 modules is constructed, it is possible to scan the entire body in less than one minute. Moreover, if a MIMO module with a substantial number of transmitting and receiving antennas is used, the scanning time will be significantly reduced, as frequent repetition of scanning becomes unnecessary.

Consequently, we could acquire 3D point cloud data enabling the construction of a seamless 3D image of the human body. Fig. 8 depicts the 3D point cloud data obtained through multi-angle scanning of the clothed human body. Fig. 8(a) displays the 3D point cloud image obtained in front of the human body, while Fig. 8(b) presents the processed 3D

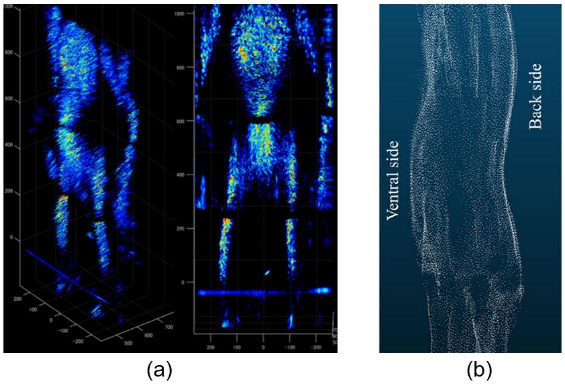

FIGURE 8. **(a) 3D point cloud image in one scanning direction after extracted peak intensity. (b) Reconstructed 3D point cloud image.**

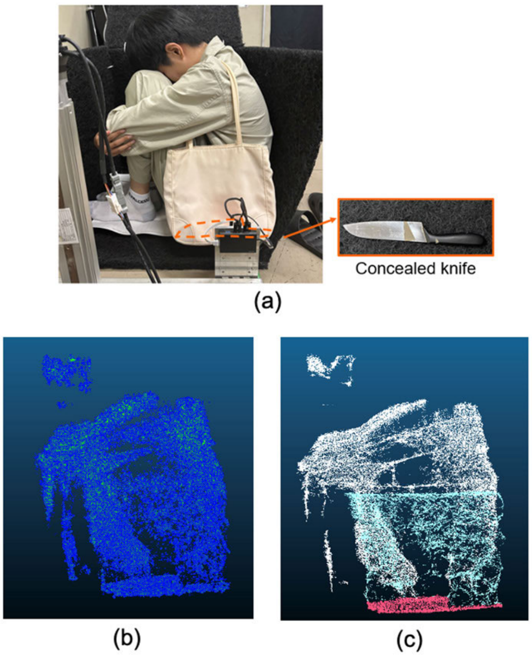

FIGURE 9. **(a) The security check sample. (b) 3D point cloud image after extracted peak intensity. (c) Reconstructed 3D point cloud image.**

point cloud image. Despite the inherent uncertainties introduced by slight variations in breathing and posture, as well as the presence of noise and potential measurement errors during the scanning process, we achieved successful 3D reconstructed images that accurately capture the distinctive features of the human body shape.

MMWs, which do not harm the human body, may also be useful in checking for weapons and other items concealed by people. As an example, we observed a person with a knife hidden in a bag, as shown in Fig. 9 (a). The extracted 3D point cloud data, obtained after extracting based on peak intensity, is shown in Fig. 9(b), The image of the human body and knife is relatively blurred. Additionally, Fig. 9(c) shows the reconstructed 3D point cloud image, where the white point cloud represents the human body, the blue point cloud signifies the reflection of the bag, and the pink point cloud indicates the concealed knife, the knife's shape is clearly discernible in this image. It can be concluded that compared to the point cloud image after extracted peak intensity, the reconstructed point cloud data can get a clearer contour of the non-flat object, and the algorithm we developed removes the noise from the 3D imaging effectively. As these results show, using our MMW scanning system and the algorithms of the 3D image reconstruction program, it is possible to make a clear distinction between the human body, the bag, and the knife (weapon).

VI. CONCLUSION

In this study, a MIMO-SAR FMCW MMW radar imaging system was constructed and the techniques to obtain accurate 2D and 3D reconstructed images using the observed point cloud data were developed. In the case of 2D reconstructed imaging, we employed 2D cross-sectional imaging at a certain distance and intensity integration imaging to visualize objects within a specific distance. For 3D imaging, we have developed a noise reduction method that facilitates the acquisition of smooth surface 3D point cloud data. These technological developments have enabled the measurement of non-planar objects and objects placed at different distances with high spatial resolution. In other words, we have succeeded in constructing an image reconstruction technique with a spatial resolution of less than 1 mm both in-plane (X-Z plane) and at a distance (Y-axis direction).

Moreover, when imaging clothed human subjects, we conducted scans from 16 different angles, successfully generating 3D reconstructed images that obtained the uneven surface of the human body. Importantly, by applying this system in security applications, we achieved the identification of dangerous items carried by a human successfully, highlighting its potential for practical implementation.

Moving forward, our future research will concentrate on utilizing the 3D point cloud data obtained from the reconstruction process for object recognition based on deep learning techniques. By doing so, we aim to enhance the efficiency and intelligence of the system, further advancing its capabilities.

ACKNOWLEDGMENT

The authors would like to thank Kazuma Konishi, Kengo Ota, and Hiroshi Otera for their assistance with the proposed system's software and hardware.

(Yaheng Wang, Jie Su, and Taiga Fukuda contributed equally to this work.)

REFERENCES

[1] J. Hasch, E. Topak, R. Schnabel, T. Zwick, R. Weigel, and C. Waldschmidt, "Millimeter-wave technology for automotive radar sensors in the 77 GHz frequency band," *IEEE Trans. Microw. Theory Techn.*, vol. 60, no. 3, pp. 845–860, Mar. 2012.

[2] S. M. Patole, M. Torlak, D. Wang, and M. Ali, "Automotive radars: A review of signal processing techniques," *IEEE Signal Process. Mag.*, vol. 34, no. 2, pp. 22–35, Mar. 2017.

[3] M. Alizadeh, G. Shaker, J. C. M. D. Almeida, P. P. Morita, and S. Safavi-Naeini, ''Remote monitoring of human vital signs using mm-wave FMCW radar,'' *IEEE Access*, vol. 7, pp. 54958–54968, 2019.

[4] Z. Yang, P. H. Pathak, Y. Zeng, X. Liran, and P. Mohapatra, ''Monitoring vital signs using millimeter wave,'' in *Proc. 17th ACM Int. Symp. Mobile Ad Hoc Netw. Comput.*, Jul. 2016, pp. 1–12.

[5] L. Chao, M. N. Afsar, and K. A. Korolev, ''Millimeter wave dielectric spectroscopy and breast cancer imaging,'' in *Proc. 7th Eur. Microw. Integr. Circuit Conf.*, Oct. 2012, pp. 572–575.

[6] T. Nagatsuma and S. Oka, ''Millimeter-wave imaging and its application to structure diagnosis,'' *NTT Tech. J.*, vol. 18, no. 6, pp. 25–28, 2006.

[7] S. Oka, H. Togo, N. Kukutsu, and T. Nagatsuma, ''Latest trends in millimeter-wave imaging technology,'' *Prog. Electromagn. Res. Lett.*, vol. 1, pp. 197–204, 2008.

[8] R. Appleby and R. N. Anderton, ''Millimeter-wave and submillimeter-wave imaging for security and surveillance,'' *Proc. IEEE*, vol. 95, no. 8, pp. 1683–1690, Aug. 2007.

[9] A. Hirata, K. Suizu, Y. Sudo, I. Watanabe, N. Sekine, and A. Kasamatsu, ''Non-destructive inspection of concrete surface crack using near-field scattering,'' in *Proc. IEEE Int. Symp. Radio-Freq. Integr. Technol. (RFIT)*, Hiroshima, Japan, Sep. 2020, pp. 244–246.

[10] W. Choi and R. Han, ''Perspective on active submillimeter electromagnetic wave imaging using CMOS integrated circuits technologies,'' *J. Appl. Phys.*, vol. 133, no. 15, pp. 1–12, Apr. 2023.

[11] A. Chopard, J.-P. Guillet, P. Gellie, B. Recur, H. Balacey, and P. Mounaix, ''Skeletonization and 3D rendering with real time terahertz tomography,'' *Opt. Continuum*, vol. 2, no. 5, p. 1060, 2023.

[12] Y. Wang, L. Yi, M. Tonouchi, and T. Nagatsuma, ''High-speed 600 GHz-band terahertz imaging scanner system with enhanced focal depth,'' *Photonics*, vol. 9, no. 12, p. 913, Nov. 2022.

[13] A. Luukanen, R. Appleby, M. Kemp, and N. Salmon, ''Millimeter-wave and terahertz imaging in security applications,'' *THz Spectrosc. Imag.*, vol. 171, pp. 491–520, Oct. 2012.

[14] X. Zhuge and A. G. Yarovoy, ''A sparse aperture MIMO-SAR-based UWB imaging system for concealed weapon detection,'' *IEEE Trans. Geosci. Remote Sens.*, vol. 49, no. 1, pp. 509–518, Jan. 2011.

[15] D. M. Sheen, D. L. Mcmakin, and T. E. Hall, ''Three-dimensional millimeter-wave imaging for concealed weapon detection,'' *IEEE Trans. Microw. Theory Techn.*, vol. 49, no. 9, pp. 1581–1592, Mar. 2001.

[16] K. Brinker, M. Dvorsky, M. T. Al Qaseer, and R. Zoughi, ''Review of advances in microwave and millimetre-wave NDT & E: Principles and applications,'' *Phil. Trans. Roy. Soc. A, Math., Phys. Eng. Sci.*, vol. 378, no. 2182, Oct. 2020, Art. no. 20190585.

[17] K. W. Tang, M. Khanpour, P. Garcia, C. Garnier, and S. P. Voinigescu, ''65-nm CMOS, W-band receivers for imaging applications,'' in *Proc. IEEE Custom Integr. Circuits Conf.*, San Jose, CA, USA, Sep. 2007, pp. 749–752.

[18] D. Rozban, A. Aharon, L. Kahana, A. Abramovich, Y. Yitzhaky, H. Altan, and N. S. Kopeika, ''Robust, sensitive, and inexpensive 2D focal plane array upconverting MMW imaging into the visible,'' *IEEE Photon. Technol. Lett.*, vol. 31, no. 10, pp. 747–750, May 15, 2019.

[19] K. Ramasubramanian and J. Singh, ''AWR1443 single-chip radar: For diverse proximity-sensing applications,'' Texas Instrum., Dallas, TX, USA, Tech. Rep., SPYY008, 2017.

[20] C. M. Watts, P. Lancaster, A. Pedross-Engel, J. R. Smith, and M. S. Reynolds, ''2D and 3D millimeter-wave synthetic aperture radar imaging on a PR2 platform,'' in *Proc. IEEE/RSJ Int. Conf. Intell. Robots Syst. (IROS)*, Oct. 2016, pp. 4304–4310.

[21] M. E. Yanik, D. Wang, and M. Torlak, ''Development and demonstration of MIMO-SAR mmWave imaging testbeds,'' *IEEE Access*, vol. 8, pp. 126019–126038, 2020.

[22] J. Gao, Y. Qin, B. Deng, H. Wang, and X. Li, ''Novel efficient 3D short-range imaging algorithms for a scanning 1D-MIMO array,'' *IEEE Trans. Image Process.*, vol. 27, no. 7, pp. 3631–3643, Jul. 2018.

[23] F. Gumbmann and L.-P. Schmidt, ''Millimeter-wave imaging with optimized sparse periodic array for short-range applications,'' *IEEE Trans. Geosci. Remote Sens.*, vol. 49, no. 10, pp. 3629–3638, Oct. 2011.

[24] A. G. Stove, ''Linear FMCW radar techniques,'' *IEE Proc. F Radar Signal Process.*, vol. 139, no. 5, p. 343, 1992.

[25] A. Meta, P. Hoogeboom, and L. P. Ligthart, ''Signal processing for FMCW SAR,'' *IEEE Trans. Geosci. Remote Sens.*, vol. 45, no. 11, pp. 3519–3532, Nov. 2007.

[26] J. Li and P. Stoica, *MIMO Radar Signal Processing*. Hoboken, NJ, USA: Wiley, 2008.

[27] R. W. Heath, N. González-Prelcic, S. Rangan, W. Roh, and A. M. Sayeed, ''An overview of signal processing techniques for millimeter wave MIMO systems,'' *IEEE J. Sel. Topics Signal Process.*, vol. 10, no. 3, pp. 436–453, Apr. 2016.

[28] M. E. Yanik and M. Torlak, ''Near-field MIMO-SAR millimeter-wave imaging with sparsely sampled aperture data,'' *IEEE Access*, vol. 7, pp. 31801–31819, 2019.

[29] G. Krieger, T. Rommel, and A. Moreira, ''MIMO-SAR tomography,'' in *Proc. 11th Eur. Conf. Synth. Aperture Radar*, Hamburg, Germany, Jun. 2016, pp. 1–6.

[30] W.-Q. Wang, ''MIMO SAR imaging: Potential and challenges,'' *IEEE Aerosp. Electron. Syst. Mag.*, vol. 28, no. 8, pp. 18–23, Aug. 2013.

[31] N. Mohammadian, O. Furxhi, R. D. Short, and R. G. Driggers, ''SAR millimeter wave imaging systems,'' *Proc. SPIE*, vol. 10994, pp. 86–98, May 2019.

[32] I. Cumming and F. H. Wong, *Digital Processing of Synthetic Aperture Radar Data: Algorithms and Implementation*. Norwood, MA, USA: Artech House, 2005.

[33] L. Qiao, Y. Wang, Z. Zhao, and Z. Chen, ''Exact reconstruction for near-field three-dimensional planar millimeter-wave holographic imaging,'' *J. Infr., Millim., THz Waves*, vol. 36, no. 12, pp. 1221–1236, Dec. 2015.

[34] F. Berizzi and G. Corsini, ''A new fast method for the reconstruction of 2-D microwave images of rotating objects,'' *IEEE Trans. Image Process.*, vol. 8, no. 5, pp. 679–687, May 1999.

[35] J. Gao, Y. Qin, B. Deng, H. Wang, and X. Li, ''A novel method for 3-D millimeter-wave holographic reconstruction based on frequency interferometry techniques,'' *IEEE Trans. Microw. Theory Techn.*, vol. 66, no. 3, pp. 1579–1596, Mar. 2018.

[36] L. Qiao, Y. Wang, Z. Zhao, and Z. Chen, ''Range resolution enhancement for three-dimensional millimeter-wave holographic imaging,'' *IEEE Antennas Wireless Propag. Lett.*, vol. 15, pp. 1422–1425, 2016.

[37] Y. Wang, ''Rotated reconstructed 3D imaging results,'' IEEE Dataport, Jul. 2023, doi: 10.21227/aqcq-6552.

[38] R. Gens and J. L. Van Genderen, ''Review article SAR interferometry—Issues, techniques, applications,'' *Int. J. Remote Sens.*, vol. 17, no. 10, pp. 1803–1835, Jul. 1996.

YAHENG WANG received the B.S. degree from the School of Mechanical Engineering and Applied Electronics Technology, Beijing University of Technology, Beijing, China, in 2020, and the M.E. degree from the Graduate School of Engineering Science, Osaka University, Osaka, Japan, in 2023, where she is currently pursuing the Ph.D. degree with the Graduate School of Engineering. Her research interest includes millimeter- and terahertz-wave imaging.

JIE SU received the B.S. degree from the School of Instrumentation of Optoelectronic Science and Engineering, Beihang University, Beijing, China, in 2019. He is currently pursuing the master's degree with the Graduate School of Engineering, Osaka University, Osaka, Japan. His research interest includes millimeter-wave imaging.

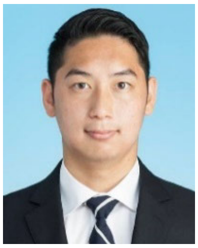

TAIGA FUKUDA received the B.S. degree from the School of Engineering, Osaka University, Osaka, Japan, in 2021, where he is currently pursuing the master's degree with the Graduate School of Engineering. His research interest includes millimeter-wave imaging.

MASAYOSHI TONOUCHI (Member, IEEE) received the B.S., M.S., and Dr.E. degrees from Osaka University, Japan, in 1983, 1985, and 1988, respectively.

From 1988 to 1989, he was with the Faculty of Engineering Science, Osaka University. From 1989 to 1994, he joined the Kyushu Institute of Technology. From 1994 to 1996, he was a Principal Researcher with the Communications Research Laboratory, Japan. From 1996 to 2000, he was an Associate Professor with Osaka University, where he has been a Full Professor with the Institute of Laser Engineering, since 2000. His current research interests include ultrafast and terahertz science in advanced materials and the application of THz technology. He has been leading the research and development of the Laser Terahertz Emission Microscope (LTEM), since 1996.

Prof. Tonouchi has been an Associated Editor of the *Journal of Applied Physics*, since 2015. He is a member of the SPIE, OSA, the Japan Society of Applied Physics, the Physical Society of Japan, and the Institute of Electronics, Information, and Communication Engineers.

HIRONARU MURAKAMI received the B.S. and M.S. degrees in physics from Kyushu University, Fukuoka, Japan, in 1984 and 1986, respectively, and the Dr.-Eng. degree in electrical engineering from Osaka University, Osaka, Japan, in 1995.

From 1988 to 2000, he was a Research Associate with the Department of Electrical Engineering, Osaka University. From August 2000 to June 2004, he was an Associate Professor with the Research Center for Superconductor Photonics, Osaka University, where he has been an Associate Professor with the Institute of Laser Engineering, since July 2004. His current research interests include the development of a terahertz spectroscopic imaging system for studying cancer at the cellular level and the non-destructive testing of infrastructure using millimeter-wave electromagnetic waves.